Research Article Vol. 58, No. 33 / 20 November 2019 / Applied Optics 9259

applied optics

Small and lightweight laser retro-reflector arrays for lunar landers

Xiaoli Sun,[1,*] David E. Smith,[2] Evan D. Hoffman,[1] Shane W. Wake,[1] Daniel R. Cremons,[3] Erwan Mazarico,[1] Jean-Marie Lauenstein,[1] Maria T. Zuber,[2] and Edward C. Aaron[4]

[1]NASA Goddard Space Flight Center, Code 698/61A/551/561, Greenbelt, Maryland 20771, USA
[2]Department of Earth, Atmospheric and Planetary Sciences, Massachusetts Institute of Technology, Cambridge, Massachusetts 02139, USA
[3]Universities Space Research Association (USRA), Columbia, Maryland 21046, USA
[4]KBRwyle Technology Solutions, LLC, Lanham, Maryland 20706, USA
*Corresponding author: xiaoli.sun-1@nasa.gov

Received 13 September 2019; accepted 22 October 2019; posted 30 October 2019 (Doc. ID 377578); published 20 November 2019

A set of small and lightweight laser retro-reflector arrays (LRAs) was fabricated and tested for use on lunar landers under NASA's Commercial Lunar Payload Service program. Each array contains eight 1.27-cm-diameter corner cube retro-reflectors mounted on a dome-shaped aluminum structure. The arrays are 5.0 cm in diameter at the base, 1.6 cm in height, and 20 g in mass. They can be tracked by an orbiting laser altimeter, such as the Lunar Orbiter Laser Altimeter, from a distance of a few hundred kilometers or by a landing lidar on future lunar landers. The LRAs demonstrated a diffraction-limited optical performance. They were designed and tested to survive and function on the Moon for decades, well after the lander missions are completed.

https://doi.org/10.1364/AO.58.009259

1. INTRODUCTION

Small laser retro-reflector arrays (LRAs) have been used for laser ranging to Earth-orbiting satellites from ground stations [1]. Three large LRAs were placed on the Moon by the Apollo astronauts and two were on the Lunokhod lunar landers. They have been used for lunar laser ranging from Earth over the past 50 years [2–4]. Small LRAs have also been considered by NASA Goddard Space Flight Center (GSFC) for use on Mars landers as fiducial markers for future laser tracking from an orbiting lidar [5–7]. One LRA by the National Space Agency of Italy (ASI, for Agenzia Spaziale Italiana) was on the ExoMars Schiaparelli module of the European Space Agency (ESA) [8]. A similar LRA from ASI was installed on NASA's Mars InSight lander for potential future laser ranging from orbit [9]. Tracking small LRAs on the ground from an orbiting lidar has been demonstrated by the Geoscience Laser Altimeter System (GLAS) on the Ice, Cloud, and Elevation Satellite (ICESat) [10]. NASA is planning to put small LRAs on future commercial lunar landers from the United States and international lunar landers for laser ranging from lunar orbiting lidar, such as the Lunar Orbiter Laser Altimeter (LOLA) onboard the Lunar Reconnaissance Orbiter (LRO), which is currently in orbit around the Moon [11,12]. A set of small LRAs has been fabricated based on the original design for the Mars Lander [5]. The arrays are 5.0 cm in diameter and 1.6 cm in height, and weigh 20 g. They have been tested to withstand the launch and landing and to remain functional on the lunar surface for decades. One of these LRAs was mounted on the Beresheet lunar lander by SpaceIL of Israel, which was launched in February 2019. Another one was mounted on the Vikram lunar lander on the Chandrayaan-2 mission by the India Space Research Organisation (ISRO), which was launched in July 2019. These LRAs will be on all lunar landers from the United States in the coming years under the NASA Commercial Lunar Payload Service (CLPS) program. In this paper, we describe the design and testing of these LRAs and the potential applications for science and exploration.

A small LRA on a lander on the Moon or an asteroid can be detected by an orbiting lidar. The LRA position on the surface can be derived from a series of range measurements from the lidar (Fig. 1). Once the location of the LRA has been established, subsequent orbiting lidar can range to the LRA to assist in the orbit determination of the host spacecraft. Over time, these laser ranging measurements could be used to monitor the tectonic movement of the landing site, if present. The LRA position can also be used to establish a local geodetic coordinate system around the lander.

The small LRAs will remain functional long after the lander has accomplished its primary mission objectives. They can continue to be used as precision landmarks for guidance and navigation during the lunar day or night. A landing lidar such as a flash lidar can detect these LRAs during descent. A few

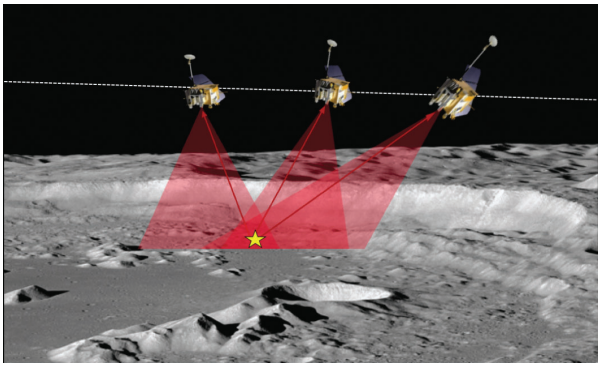

Fig. 1. Laser ranging from an orbital lidar to determine the lander position on the lunar surface, and help the orbiter to self-determine its trajectory once the position of the lander is established.

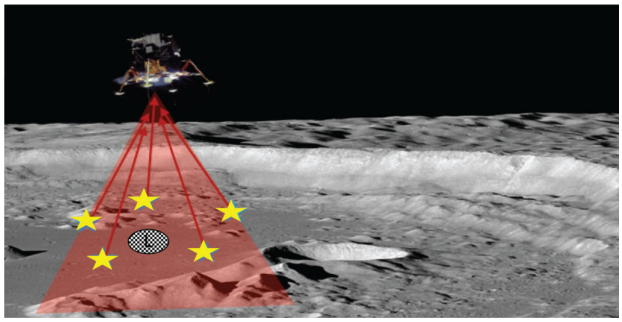

Fig. 2. Laser ranging to a number of LRAs as precision landmarks for safe landing by follow-on landers.

LRAs surrounding the landing site can serve as precision landmarks to guide the arriving landers. Figure 2 shows how a few LRAs surrounding a targeted landing area could be used to help autonomous and safe landing.

Small LRAs can also be deployed as fiducial markers on asteroids, similar to the target markers deployed on the asteroid 162173 Ryugu by the Hayabusa2 spacecraft [13–15]. One possible configuration is to attach two of these LRAs at the base in a spheroid shape such that one side always faces up regardless how the joined arrays land on the asteroid surface. They can then be tracked by an orbiting or co-orbiting spacecraft with a lidar to precisely measure the rotational parameters (spin axis and rate) and other geophysical properties of the asteroid, as depicted in Fig. 3.

Although these LRAs are small, they have a relatively large equivalent optical cross section (10^4 to 10^5 m^2) and can be tracked by a lidar from a few hundred kilometers distance, as described in Section 5. They produce a distinct return that can be uniquely identified from the surface returns by the return pulse amplitude and shape, as demonstrated by ICESat [10]. It may take several orbital passes for it to be located with current topographic lidar, such as LOLA, which has a small laser footprint size and low pulse rate. They are expected to be located much more easily by future swath mapping lidar with contiguous or overlapping laser footprints in a push-broom measurement configuration.

It should be noted that these small LRAs are designed for laser ranging from a lunar orbiting lidar to the lunar lander but not from Earth directly. The retro-reflectors on these LRAs are about 1/3 the size of those on the Apollo LRAs, and they are oriented in different directions of the sky instead of all pointed to Earth. The Apollo LRAs have 100 to 300 retro-reflectors contributing to the return signal at the same time, compared to one retro-reflector at a time by these small LRAs. The received signal from these small LRAs is $\ll 0.1\%$ of the signal from the Apollo LRAs. At present, the highest received signal levels from the Apollo LRAs is six to seven detected photons per laser pulse at the Apache Point Observatory [16]. Thus, it is not practical with today's technology to range to these small LRAs directly from Earth-based stations. Nevertheless, these small LRAs are expected to be as durable as the Apollo and Lunokhod LRAs, and they will be taken to different parts of the Moon by the new lunar landers.

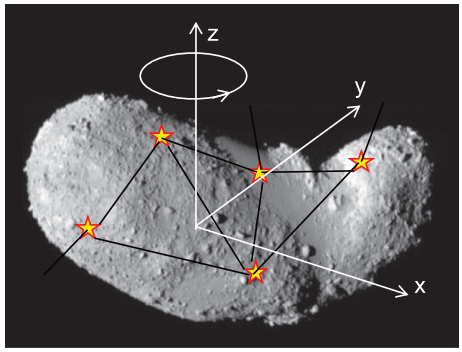

Fig. 3. Deployable LRAs on an asteroid for laser ranging from an orbiting or co-orbiting spacecraft with a lidar to determine its orientation, rotation axis, etc.

There are unique technical challenges for the LRAs on lunar landers compared to those on Earth-orbiting satellites or Mars landers. First, they have to be small and lightweight so that they can be carried to the Moon by lunar landers from the NASA CLPS program. Second, they have to remain functional over the entire lunar surface temperature range, 85 K to 385 K (−189°C to 111°C) [17], which is a much wider temperature range compared to LRAs on Earth-orbiting satellites and landers on Mars. Third, they are exposed to the sky without shielding and have to survive a much higher dose of space radiation and for a much longer period of time than those required for most spacecraft components.

2. LASER RETRO REFLECTOR ARRAY DESIGN

The LRAs were originally designed in the early 2000s for the Phoenix Mars Lander for ranging from an orbiting lidar (also known as a laser altimeter) similar to the Mars Orbiter Laser Altimeter (MOLA) [5,6,18]. They were specially designed for low mass and a near-full sky view. Each LRA consists of eight 1.27-cm-diameter solid retro-reflectors (also known as corner cubes or cube-corners) mounted on a dome-shaped aluminum structure, as shown in Fig. 4. Each retroreflector has a maximum useful light incidence angle of about ±20° [19–22]. Four retro-reflectors are evenly distributed on a ring 20° from zenith and the other four on a ring 40° from zenith. Therefore, the entire LRA can be ranged to from any direction 30° above the horizon.

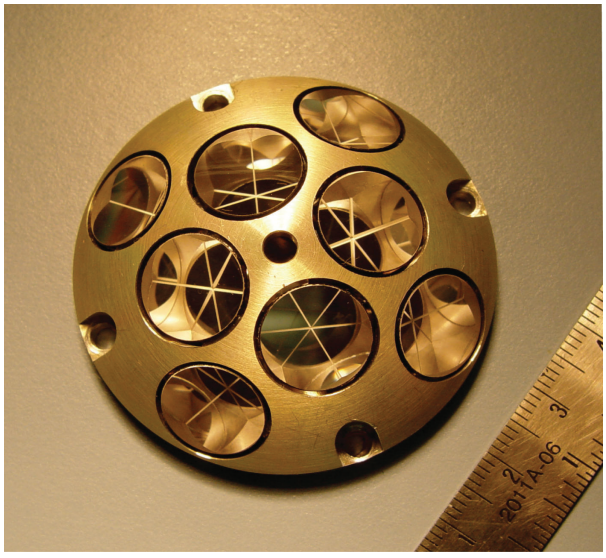

Fig. 4. Photograph of the LRA. It is 5.0 cm in diameter at the base and 1.6 cm in height, and weighs 21 g.

The retro-reflectors are made of a special type of quartz called Suprasil, which has a high optical homogeneity in all three axes and is proven to be radiation resistant. The index of refraction is about 1.46, varying slightly with the wavelength. To reduce the mass, the retro-reflectors are bonded to the aluminum structure instead of mechanically constrained as they are for most Earth orbiting satellites. A standard chromate-conversion coating (Iridite) was used for the aluminum structure for corrosion resistance and high electrical conductivity to prevent the build up of static electrical charges on the LRA in space and on the Moon. The mass of the LRA is 20 ± 1 g, not including fasteners. The original LRA designed for the Mars lander used plated retro-reflectors with the three exterior facets of the corner cubes mirror-coated with aluminum. The recent LRAs for commercial and international lunar landers use non-plated or total internal reflection (TIR), retro-reflectors. Although TIR retro-reflectors have a slightly narrower light acceptance angle and the return is affected by the polarization of the incident light [23], they have a simpler design. They are less susceptible to thermal distortion and likely to have a longer lifetime on the Moon. The size of the retro-reflectors was chosen to maintain low mass but still give a sufficient cross section for laser ranging from an orbiting spacecraft. The small size and low mass also help to minimize thermal gradients across the retro-reflector under solar illumination, which are known to cause degradation in optical performance [24].

3. OPTICAL PERFORMANCE TESTING

The key parameters that govern the optical performance of the retro-reflectors are the dihedral angles and the surface flatness. They were measured by the retro-reflector supplier and verified at NASA GSFC using interferometers. The average dihedral angles were measured to be about 0.3 arcseconds root-mean-squares (rms), which is adequate to maintain the optical losses to within 30% [25]. The surface flatness is within 1/10 the laser wavelength at 633 nm. The dihedral angles and surface flatness of one retro-reflector were also measured from 100 K to 375 K in 20 K steps, and there were no measurable changes over this temperature range.

The far-field patterns of the retro-reflected beams were characterized at NASA GSFC using a 2.5-m focal length collimator and camera system at about 2.1 μrad per pixel resolution. The test setup was calibrated against a gold-coated mirror of the same clear aperture and positioned normal to the incidence laser beam. A sample far-field pattern from a single retro-reflector is shown in Fig. 5. The divergence of the center lobe of the retro-reflected beam was measured to be 156 μrad full-angle at 1064-nm wavelength, and the acceptance angle was about ±20°.

Additional optical performance tests were performed, and the full results will be reported in a separate publication. These include the dihedral angles and surface flatness of a sample set of single retro-reflectors, dihedral angles and surface flatness of a single retro-reflector versus temperature, far-field patterns from

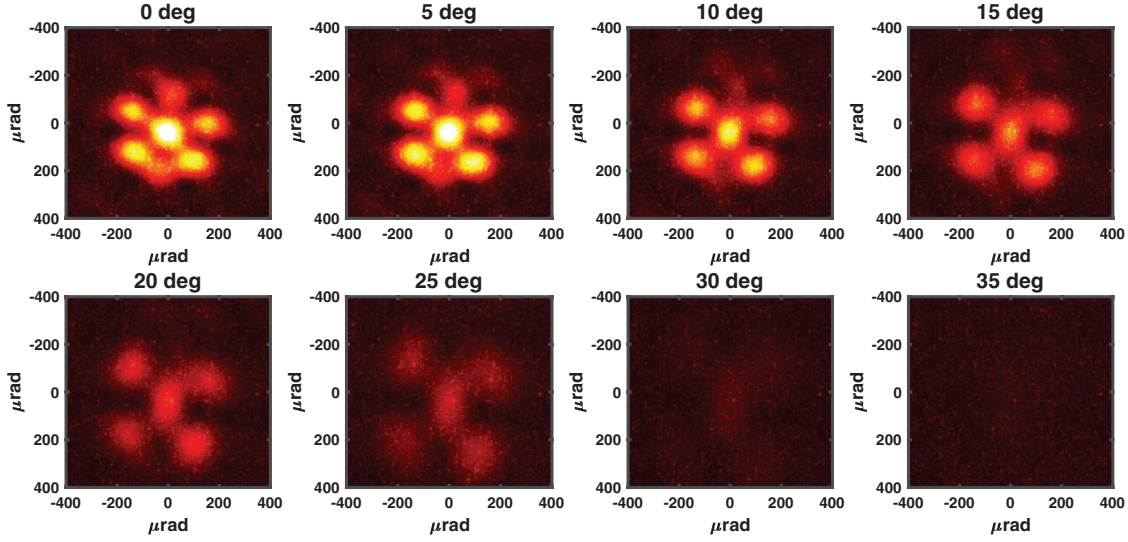

Fig. 5. Far-field pattern of a TIR retro-reflector at 1064-nm laser wavelength as a function of incidence angle.

single and multiple retro-reflectors versus incidence angle, far-field patterns at different laser wavelengths and polarizations, and the pulse shapes of the retro-reflected laser light at different incidence angles.

4. ENVIRONMENTAL TESTING

Several environmental tests were performed on the LRAs to verify that they can withstand the vibrations during launch and landing, the temperature range during cruise and on the lunar surface from day to night, and the lunar radiation environment for several decades. A qualification unit was built using the same procedure and materials for some of the tests to avoid unnecessary stress and wear to the flight units. The following subsections give the details of the vibration, thermal vacuum, and radiation testing of the LRAs at NASA GSFC before delivering them to the lunar landers.

A. Vibration Tests

Vibration tests were performed according to the NASA Standards and the lander-specific requirements. There were two sets of vibration tests conducted: qualification and acceptance tests. The former were performed on the qualification unit to the full vibration levels, including a random vibration test to 26 g rms, a sine sweep test to 100 Hz, and a shock response test to 2000 g. The acceptance tests were performed on all the flight LRAs to verify workmanship per NASA GSFC General Environmental Verification Standard GSFC-STD-7000. The vibration specification for the qualification unit and the flight units are given in Tables 1 through 4, with the z axis defined to be normal to the LRA base. The LRAs passed all the vibration tests. A static load test was performed on the qualification unit after the vibration tests, and the bond strength between the corner cube retro-reflectors and the aluminum support structure was found to meet the requirement with margin. No resonances were found over the entire test frequency range.

Table 1. Random Vibration Test Level—Qualification

All Three Axes	
20 Hz	0.04 g^2/Hz
80–300 Hz	1.5 g^2/Hz
300–1300 Hz	0.3 g^2/Hz
1300–300 Hz	1.5 g^2/Hz
Overall level	26 g rms
Duration	2 min per axis

Table 2. Sine Vibration Test Level—Qualification

Frequency	*Z* axis	*X* and *Y* Axes
5–20 Hz	8.3 g	8.3 g
20–50 Hz	13.3 g	13.3 g
50–100 Hz	60 g	30 g
Sweep rate	3–4 octaves/min	3–4 octaves/min

Table 3. Shock Response Test—Qualification

Frequency	*Z* axis	*X* and *Y* Axes
100 Hz	30 g	30 g
1500 Hz	2000 g	2000 g
10,000 Hz	2000 g	2000 g

Table 4. Random Vibration Test Level—Workmanship

All Three Axes	
20 Hz	0.013 g^2/Hz
20–50 Hz	+6 dB/octave
50–800 Hz	0.08 g^2/Hz
800–2000 Hz	+6 dB/octave
2000 Hz	0.013 g^2/Hz
Overall level	10 g rms
Duration	1 min per axis

B. Thermal Vacuum Tests

A thermal cycle test was performed for every flight LRA in vacuum over a temperature range of 85 K to 385 K. The LRAs were tested in a liquid nitrogen Dewar with an adapter plate and a set of heaters, as shown in Fig. 6. The LRAs were held at the hot and cold temperatures for at least 8 h. The rate of temperature transition was about 3 K/min. There were a total of five temperature cycles for each LRA. Figure 7 shows the temperature profile of the test.

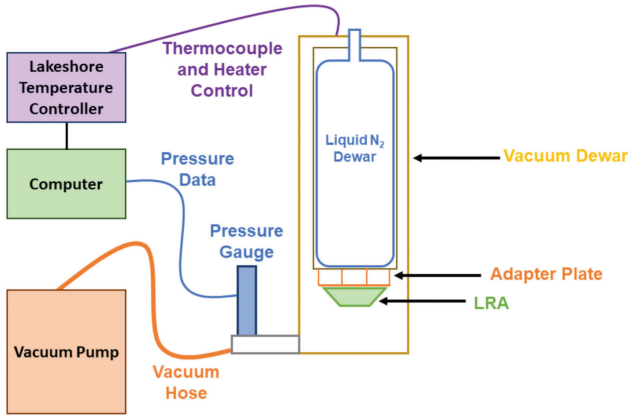

Fig. 6. LRA thermal vacuum test setup.

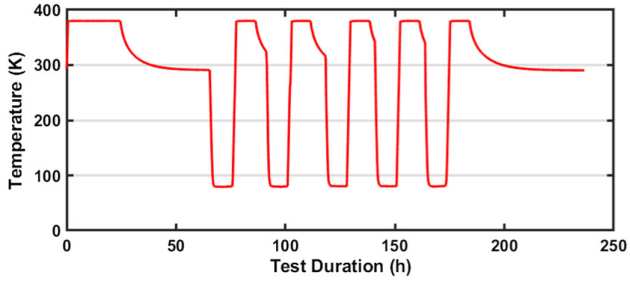

Fig. 7. Temperature profile of the thermal vacuum tests of the LRAs.

All LRAs passed the thermal vacuum tests. There were no noticeable changes after the tests, except for a slight fading of the Iridite coating on the aluminum surface. Slight discoloring of Iridite is expected under high temperature and vacuum but should still provide enough corrosion resistance for the LRAs during handling and storage on Earth. It should have no effect on their lifetime on the lunar surface [26]. Detailed examination of the Iridite coating under a high-power microscope showed no metal damage. The bonding strength between the retro-reflectors and the aluminum structure of the qualification unit was also tested after the temperature cycle test, and it met the specification with margin.

C. Radiation Damage Tests

Since the LRAs are likely to be mounted on the top deck of the landers, they will receive the full space radiation incident on the lunar surface. Most of the concerns about radiation damage to these LRAs were related to the bonding material, which had not been tested to such a high radiation level. Another radiation damage mechanism to be considered is the darkening of the glasses used for the retro-reflectors. The objective of the test was to demonstrate a useful lifetime of several decades so that they can be ranged to by future lunar lidar.

The LRAs are exposed to space radiation on the top and shielded by the Moon on the bottom. The primary radiation is from solar protons when the LRAs are on the sunlit side of the Moon. Protons cause both ionization damage and displacement damage to the materials. For optics such as the retro-reflectors, the major radiation damage results from the proton-induced ionizing dose that causes darkening of the material [27,28]. Since the retro-reflectors are not shielded, most of the ionizing energy is deposited by low-energy protons that are absorbed in the top layer of the material. Gamma rays are often used to test the ionizing radiation damage susceptibility of optical materials because they are more accessible and have lower cost compared to proton accelerators. For the same amount of dose, gamma rays have been shown to have a greater impact on transmission loss in glass as compared to protons [29,30], thereby providing a more conservative test.

The ionizing dose on the lunar surface over a 10-year period was calculated at the 95% confidence level as a function of aluminum shielding thickness using the Emission of Solar Protons (ESP) model and both the NOVICE and SHIELDOSE software packages. The results are shown in Fig. 8. An additional 10% of the total direct dose is added to account for the reflected particles by the lunar surface onto the lunar lander. The total ionizing dose averaged over 10 years is expected to be 8.8 Mrad(Si) based on the NOVICE result, which is much higher than what most of the spacecraft components are designed for. The adhesive that holds the retro-reflectors to the support structure is mostly behind the aluminum shell and can be assumed to have an equivalent of 1-mm aluminum shielding. The expected dose for the adhesives is below 0.1 Mrad(Si) over 10 years based on Fig. 8.

A gamma-ray radiation test was conducted on the qualification unit of the LRA using a Cobalt-60 source. The adhesive and the assembly procedure of the qualification unit were exactly the same as the flight unit, though the retro-reflectors were made of

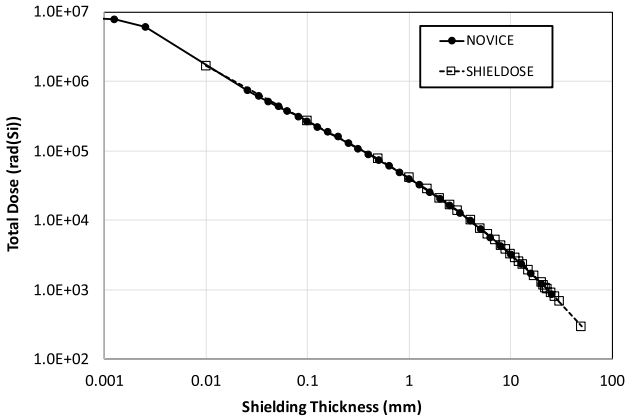

Fig. 8. Average total ionization dose on the lunar surface over 10 years.

a similar type of quartz but not the Suprasil used on the flight units. The total dose of the test was 17.8 Mrad(Si) at a dose rate of about 2 krad(Si)/min, which is equivalent to about a 20-year exposure to the space radiation on the lunar surface with essentially no shielding according to Fig. 8. The integrity of the adhesives and the clearness of the retro-reflectors were examined periodically during the test, and no change was observed except for a slight hardening of the adhesives. A static load test of the retro-reflectors was performed by applying a static force up to 50 times the required retention strength of the adhesive for each of the eight retro-reflectors on the array. The LRA showed no observable differences before or after the radiation test. A single flight-spare retro-reflector was also tested to 13.7 Mrad(Si), and again there was no change found when compared to an identical but nonirradiated retro-reflector. Based on these results, the adhesives should survive the radiation on the lunar surface for many decades. The LRAs are predicted to have no degradation in optical performance for two decades and remain functional for more decades to come on the lunar surface.

5. LASER RANGING TO THE LRAs

Link equation. The received signal from a single retro-reflector can be calculated using the link equation as [1]

$$n_s = \eta_d \eta_t \eta_r \frac{\lambda}{hc} E_t G_t(\theta_L, \delta\theta_t) \sigma_x(\theta_i) \frac{1}{(4\pi R^2)^2} A_r, \quad (1)$$

where n_s is the average number of photoelectrons recorded by the detector, η_d is the detector quantum efficiency, η_t and η_r are the transmitter and receiver optical transmission efficiencies, respectively, λ is the laser wavelength, h is Planck's constant, c is the speed of light, E_t is the transmitted laser pulse energy, $G_t(\theta_L, \delta\theta_t)$ is the transmitter antenna gain as a function of the laser beam divergence angle θ_L and the laser transmitter pointing error $\delta\theta_t$, $\sigma_x(\theta_i)$ is the equivalent cross section of the retro-reflector as a function of the laser beam incidence angle θ_i, A_r is the receiver telescope light collecting aperture area, and R is the distance from the lidar to the LRA.

The antenna gain for a Gaussian laser beam with a divergence angle of θ_L, half-angle at $1/e^2$ points, can be written as

$$G_t(\theta_L, \delta\theta_t) = \frac{8}{\theta_t^2}\, e^{-2\left(\frac{\delta\theta_t}{\theta_L}\right)^2}. \tag{2}$$

The peak cross section for a plated retro-reflector under normal incidence can be approximated as [1]

$$\sigma_{xp} = \frac{\pi^3 \rho \phi_c^4}{4\lambda^2}, \tag{3}$$

where ρ is the reflectivity, and ϕ_c is the diameter of corner cube retro-reflector. The reflectivity is typically $\rho = 78\%$ for an aluminum-plated corner cube retro-reflector. For TIR retro-reflectors, an elliptical polarization is induced into the beam as the light travels inside the retro-reflector. The phase contributions from all six unique paths through the retro-reflector (two paths for each facet of the cube) interfere with one another, changing the overall amplitude and shape of the return. The peak optical cross section for a TIR retro-reflector is 26.4% that of a perfect reflector of the same size [23].

The far-field diffraction pattern (FFDP) of the retro-reflected beam in terms of the light intensity versus the retro-reflected angle can be approximated by the Airy function

$$\sigma_x(\theta_i) = \sigma_{xp} \cdot \left[\frac{J_1\left(\frac{\pi D_c}{\lambda}\theta_i\right)}{\frac{\pi D_c}{\lambda}\theta_i}\right]^2, \tag{4}$$

where $J_1(x)$ is the Bessel function of the first kind of order one. The first null point (half-angle) is given by

$$\theta_0 = 1.22\frac{\lambda}{\phi_c}. \tag{5}$$

For the corner cubes, we used ($\phi_c = 1.27$ cm); the center lobe size is about 50 μrad and 100 μrad in radius at 532 nm and 1064 nm laser wavelengths, respectively.

When the light incidence angle is not normal to the face of the corner cube, the cross section decreases with the angle of incidence as [1,31]

$$\sigma_x(\theta_i) = \sigma_{xp}\left(\frac{2\cos\theta_i}{\pi}\right)^2 \cdot \left\{\sin^{-1}\left[\sqrt{1 - 2\,\tan^2\left(\sin^{-1}\left(\frac{\sin\theta_i}{n}\right)\right)}\right] - \sqrt{2}\,\tan\left[\sin^{-1}\left(\frac{\sin\theta_i}{n}\right)\right]\right\}^2, \tag{6}$$

where n is the index of refraction of the material used for the corner cube. The equation above accounts for both the geometric reduction of the laser light captured by the retro-reflector at oblique incidence angle and the refraction of the laser light entering the retro-reflector.

For a TIR corner cube, the cross section depends not only on the incidence angle but also on the polarization and the orientation of the corner cube [23]. The cross section versus the incident angle has to be calculated numerically [19,20]. The cross sections of TIR retro-reflectors generally have a smaller acceptance angle compared to plated retro-reflectors. The useful incidence angle is about ±20°, but can be up to ±35° at a certain orientation.

Velocity aberration. Another major factor to consider is the velocity aberration. Because the lidar on the spacecraft is moving but the return beam is retro-reflected to where the laser pulse was transmitted, the spacecraft is no longer at the peak of the retro-reflected beam by the time the retro-reflected laser pulses return. As a result, the received signal becomes lower than that given by Eqs. (1) through (6). The angles of the retro-reflected beam can be calculated as [32]

$$\theta_r = \cos^{-1}\left[\frac{(1-\alpha^2)\cos(\theta_{sc})}{1+\alpha^2+2\alpha\,\sin(\theta_{sc})\cos(\phi_{sc})}\right],$$
$$\phi_r = \tan^{-1}\left[\frac{(1-\alpha^2)\sin(\theta_{sc})\cos(\phi_{sc})}{\alpha+\sin(\theta_{sc})\cos(\phi_{sc})}\right], \tag{7}$$

and

$$\alpha = \frac{2v_{sc}}{c}, \tag{8}$$

where θ_r and ϕ_r are the angles of the reflected beam, θ_{sc} and ϕ_{sc} are the angles of the transmitted laser beam, all in the polar coordinate system in reference to the spacecraft position, and v_{sc} is the spacecraft velocity. The angle differences between the incident and the reflected beam angles, $\Delta\theta_r = \theta_r - \theta_{sc}$ and $\Delta\phi_r = \phi_r - \phi_{sc}$, respectively, give the angular deviation from the peak of the retro-reflected beam. The parameter α given in Eq. (8) is often used as a close approximation to these angular deviations.

For the 1.27-cm-diameter retro-reflector at 10° in the along-track and cross-track directions (i.e., $\theta_{sc} = \phi_{sc} = 10°$) and a typical spacecraft velocity in lunar orbit (1.6 km/s), the angular deviations are $\Delta\theta_r = 9.71$ μrad and $\Delta\phi_r = 10.0$ μrad, which is about 10% the half-angle of the retro-reflected beam divergence at 1064-nm laser wavelength. Therefore, the effect of velocity aberration is usually not a major factor for laser ranging to these small laser retro-reflectors from a lidar in a typical lunar orbit.

Maximum ranging distance. The maximum ranging distance from the spacecraft to these laser retro-reflector arrays on the lunar landers can be estimated using the above equations once the instrument parameter values are known. As an example, we consider using LOLA to range to these retro-reflectors with the relevant parameters listed in Table 5 [11]. For a $\theta_{sc} = \phi_{sc} = 10°$ and assuming only one retro-reflector is contributing to the return signal, the maximum ranging distance is 300 km when LOLA is operating at its full laser pulse energy. The LOLA laser pulse energy has been decreasing over time, and the far-field beam pattern has been degrading to multiple spatial modes [12,33]. The current LOLA laser output pulse energy is estimated to be 1/10 of the original value, and the maximum ranging distance to these laser retro-reflectors is about 170 km. The major challenge for LOLA to range to these LRAs is the targeting of its laser beam to the LRAs. Since LOLA was designed for surface topography measurements, the laser beam divergence angle was designed for high spatial resolution instead of wide coverage. The laser pulse rate is 28 Hz due to the constraints on the electrical power. LOLA samples the lunar surface with five 5-m-diameter laser spots at 25-m spacing from a 50-km orbit altitude and could easily miss the

Table 5. LOLA Instrument Parameters

Parameters	Symbols	Values
Laser pulse energy	E_t/beam	3.3 mJ into five beams
Divergence angle	θ_L	100 μrad
Wavelength	λ	1064 nm
Detector quantum efficiency	η_d	40%
Transmitter optical transmission	η_t	95%
Receiver telescope diameter	ϕ_{tel}	0.14 m
Receiver optical transmission	η_r	70%
Laser pointing error	$\delta\theta_t$	15 μrad
Retro-reflector diameter	ϕ_c	1.27 cm
Minimum detectable signal	—	90 photoelectrons/pulse
Retro-reflector optical efficiency	ρ	25%
Spacecraft velocity	v_{sc}	1.6 km/s

laser retro-reflector on any given pass. Furthermore, the laser beam pointing is controlled by the spacecraft body pointing, which has a relatively large uncertainty in real time during the maneuver and could miss the LRAs on a given pass. Therefore repeated attempts are required in order for LOLA to range to these small LRAs on the lunar surface. These difficulties can be overcome by future lunar lidar with higher sensitivity and pixelated detectors and contiguous ground coverage.

6. SUMMARY

A set of small and lightweight LRA was fabricated and tested for use on lunar landers under CLPS program. Each LRA contains eight 1.27-cm-diameter corner cubes on a dome-shaped aluminum structure. The LRA is 5.0 cm in diameter at the base, 1.6 cm in height, and 20 g in mass. The LRAs were designed and tested to survive the vibration during launch and landing. They were tested over the extreme temperature range of the lunar surface, from 85 K to 385 K. They were also tested with gamma rays to a total dose of 17.8 Mrad(Si) and showed no measurable damage. The LRAs demonstrated a near diffraction-limited far-field pattern from the optical performance tests. These LRAs can be tracked by a LOLA-like orbiting laser altimeter from a few hundred kilometers distance, or by a lidar on a lunar lander during descent. These LRAs mounted on the lunar landers are expected to remain functional and serve as fiducial marks on the Moon for many decades to come.

Funding. National Aeronautics and Space Administration (NASA) Commercial Lunar Payload Services (CLPS); NASA Postdoctoral Program (NPP), administered by Universities Space Research Association (USRA) .

Acknowledgment. We thank many people at NASA Goddard Space Flight Center for helping manage the program and deliver the LRAs over a short time period, including Michael Amato, Lisa Kelly, Robert Steele, and Jan McGarry. We thank the engineers who conducted the LRA testing, including Zachary Denny, Pete Dogoda, Ray Disilvestre, Billy Mamakos, and Hali Flores. We thank our summer intern, Zachary Taylor, for processing the radiation test data. Finally, we thank Scott Wetzel and Paul Christopoulos of KBRwyle Technology Solutions, LLC, for the fabrication and test of the LRAs.

Disclosures. The authors declare no conflicts of interest.

REFERENCES

1. J. J. Degnan, "Millimeter accuracy satellite laser ranging: a review," in *Contributions of Space Geodesy to Geodynamics: Technology*, D. E. Smith and D. L. Turcotte, eds. (American Geophysical Union, 1993), Vol. **25**, pp 133–161.
2. P. L. Bender, D. G. Gurrie, R. H. Dicke, D. H. Eckhardt, J. E. Faller, W. M. Kaula, J. D. Mulholland, H. H. Plotkin, S. K. Poultney, E. C. Silverbert, D. T. Wilkinson, J. G. Williams, and C. O. Alley, "The lunar laser ranging experiment," Science **182**, 229–238 (1973).
3. J. O. Dickey, P. L. Bender, J. E. Faller, X. X. Newhall, R. L. Ricklefs, J. G. Ries, P. J. Shelus, C. Veillet, A. L. Whipple, J. R. Waint, J. G. Williams, and C. F. Yoder, "Lunar laser ranging: a continuing legacy of the Apollo program," Science **265**, 482–490 (1994).
4. T. W. Murphy, Jr., E. G. Adelberger, J. B. R. Battat, C. D. Hoyle, N. H. Johnson, R. J. McMillan, E. L. Michelsen, S. W. Stubbs, and H. E. Swanson, "Laser ranging to the lost Lunokhod-1 reflector," Icarus **211**, 1103–1108 (2011).
5. "NASA stennis solicitation: Phoenix Mars Scout Lander retroreflector arrays," 2019, http://spaceref.com/news/viewsr.html?pid=20608.
6. M. T. Zuber, D. E. Smith, S. C. Solomon, D. O. Muhleman, J. W. Head, J. B. Garvin, J. B. Abshire, and J. L. Bufton, "Mars observer laser altimeter investigation," J. Geophys. Res. **97**, 7781–7797 (1992).
7. D. E. Smith, M. T. Zuber, H. V. Frey, J. B. Garvin, J. W. Head, D. O. Muhleman, G. H. Pettengill, R. J. Phillips, S. C. Solomon, H. J. Zwally, W. B. Banerdt, T. C. Duxbury, M. P. Golombek, F. G. Lemoine, G. A. Neumann, D. D. Rowlands, O. Aharonson, P. G. Ford, A. B. Ivanov, G. L. Johnson, P. J. McGovern, J. B. Abshire, R. S. Afzal, and X. Sun, "Mars Orbiter Laser Altimeter (MOLA): experiment summary after the first year of global mapping of Mars," J. Geophys. Res. **106**, 23689–23722 (2001).
8. S. Dell'Annello, G. D. Monache, L. Porcelli, A. Boni, S. Contessa, E. Ciocci, M. Martini, M. Tibuzzi, N. Intaglietta, L. Salvatori, P. Tuscano, G. Patrizi, G. Bianco, R. Mugnuolo, and C. Cantone, "INRRI-EDM/2016: the first laser retroreflector on the surface of Mars," Adv. Space Res. **59**, 645–655 (2017).
9. S. Dell'Annello, D. Currie, E. Ciocci, S. Contessa, G. D. Monache, R. March, M. Martini, C. Mondaini, L. Porcelli, L. Salvatori, M. Tibuzzi, G. Bianco, R. Vittori, J. Chandler, T. Murphy, M. Maiello, M. Petrassi, and A. Lomastro, "Lunar, cislunar, near/farside laser retroreflectors for the accurate: position of landers/rovers/hoppers/orbiters, commercial georeferencing, test of relativistic gravity and metrics of the lunar interior," in *Annual Meeting of the Lunar Exploration Analysis Group (LEAG)*, Columbia Maryland, USA, October 10-12, 2017, paper 5070.
10. L. Magruder, E. Silverberg, C. Webb, and B. Schutz, "In situ timing and pointing verification of the ICESat altimeter using a ground-based system," Geophys. Res. Lett. **32**, L21S04 (2005).
11. D. E. Smith, M. T. Zuber, G. B. Jackson, J. F. Cavanaugh, G. A. Neumann, H. Riris, X. Sun, R. S. Zellar, C. Coltharp, J. Connelly, R. B. Katz, I. Kleyner, P. Liiva, A. Matuszeski, E. M. Mazarico, J. F. McGarry, A. M. Novo-Gradac, M. N. Ott, C. Peters, L. A. Ramos-Izquierdo, L. Ramsey, D. D. Rowlands, S. Schmidt, and V. S. Scott, III, G. B. Shaw, J. C. Smith, J. P. Swinski, M. H. Torrence, G. Unger, A. W. Yu, and T. W. Zagwodzki, "The Lunar Orbiter Laser Altimeter investigation on the lunar reconnaissance orbiter mission," Space Sci. Rev. **150**, 209–241 (2010).
12. D. E. Smith, M. T. Zuber, G. A. Neumann, E. Mazarico, F. G. Lemoine, J. W. Head, III, P. G. Lucey, O. Aharonson, M. S. Robinson, X. Sun,

M. H. Torrence, M. K. Barker, J. Oberst, T. C. Duxbury, D. Mao, O. S. Barnouin, K. Jha, D. D. Rowlands, S. Goossens, D. Baker, S. Bauer, P. Gläser, M. Lemelin, M. Rosenburg, M. M. Sori, J. Whitten, and T. Mcclanahan, "Summary of the results from the Lunar Orbiter Laser Altimeter after seven years in lunar orbit," Icarus **283**, 70–91 (2017).
13. T. Mizuno, T. Kase, T. Shiina, M. Mita, N. Namiki, H. Senshu, R. Yamada, H. Noda, H. Kunimori, N. Hirata, F. Terui, and Y. Mimasu, "Development of the laser altimeter (LIDAR) for Hayabusa2," Space Sci. Rev. **208** 33–47 (2017).
14. https://phys.org/news/2019-06-hayabusa2-marker-asteroid-ryugu.html, last accessed on 8/1/2019.
15. S. Dell'Agnello, G. O. D. Monache, L. Porcelli, M. Tibuzzi, L. Salvatori, C. Mondaini, M. Muccino, M. D. P. Emilio, R. March, L. Loppi, O. Luongo, S. Casini, G. Bianco, D. G. Currie, R. Vittori, C. Benedetto, F. Pasquali, M. Petrassi, F. Filomena, L. Mauro, L. Rubino, and V. Sanclimenti, "Laser retroreflectors for: Dydimos, comets, Phobos, Deimos, CLPS, and lunar Lagrangian L1 for exploration, planetary and gravity science," NASA Exploration Science Forum NESF2019-038 (NASA Ames Research Center, 2019), available at https://nesf2019.arc.nasa.gov/abstract/NESF2019-038, last accessed 8/2/2019.
16. T. W. Murphy, E. G. Adelberge, J. B. Battat, L. N. Carey, C. D. Hoyle, P. LeBlanc, E. L. Michelsen, K. Nordtvedt, A. E. Orin, J. D. Strasburg, C. W. Stubbs, H. E. Swanson, and E. Willams, "The Apache point observatory lunar laser-ranging operation: instrument description and first detections," Publ. Astron. Soc. Pac. **120**, 20–37 (2008).
17. J.-P. Williams, D. A. Paige, B. T. Greenhagen, and E. Sefton-Nash, "The global surface temperatures of the Moon as measured by the diviner lunar radiometer experiment," Icarus **283**, 300–325 (2017).
18. J. B. Abshire, X. Sun, and R. Afzal, "Mars Orbiter Laser Altimeter: receiver model and performance analysis," Appl. Opt. **39**, 2449–2460 (2000).
19. D. A. Arnold, "Optical and infrared transfer function of the LAGEOS retroreflector array," NASA-CR-157182 (Smithsonian Astrophysical Observatory, 1975), available at https://ntrs.nasa.gov/archive/nasa/casi.ntrs.nasa.gov/19780017949.pdf, last accessed 6/24/2019.
20. J. W. Siry, "The LAGEOS System," NASA Technical MemorandumNASA-TM-X-73072 (NASA, 1975), available at https://ntrs.nasa.gov/archive/nasa/casi.ntrs.nasa.gov/19760006091.pdf, last accessed 6/24/19.
21. A. Marki, "Lunar laser ranging: a review," arXiv:1805.05863 [astro-ph.IM] (2018).
22. A. Egidi, "Review of main optical retroreflectors," Technical Report 31/2018 (INRIM Istituto Mazionale di Ricerca Metrologica, 2018).
23. T. W. Murphy, Jr. and S. D. Goodrow, "Polarization and far-field diffraction patterns of total internal reflection corner cubes," Appl. Opt. **52**, 117–126 (2013).
24. S. D. Goodrow and T. W. Murphy, Jr., "Effects of thermal gradients on total internal reflection corner cubes," Appl. Opt. **51**, 8793–8799 (2012).
25. Y. He, Q. Liu, H. Duan, J. He, Y. Jiang, and H. Yeh, "Manufacture of a hollow corner cube retroreflector for the next generation of lunar laser ranging," Res. Astron. Astrophys. **18**, 136 (2018).
26. M. Rodriguez, "Chromate conversion coating: Iridite 14-2 thermal/optical characterization," Proc. SPIE **8492**, 849202 (2012).
27. M. Fruit, A. Gusarov, F. Berghmans, D. Doyle, and G. Ulbrich, "Radiation impact on the characteristics of optical glasses," Proc. SPIE **10569**, 105691R (2017).
28. M. R. Ioan, I. Gruia, G. V. Ioan, L. Rusen, C. D. Negut, and P. Ioan, "The influence of gamma rays and protons affected optical media on a real Gaussian laser beam parameters," Rom. Rep. Phys. **67**, 508–522 (2015).
29. P. Silverglate, E. Zalewski, and P. Petrone, "Proton induced radiation effects on optical glasses," Proc. SPIE **1761**, 46–57 (1992).
30. M. Fruit, A. Gusarov, and D. Doyle, "Measuring space radiation impact on the characteristics of optical glasses; measurement results and recommendations from testing a selected set of materials," Proc. SPIE **4823**, 132–141 (2002).
31. P. O. Minott, "Design of retrodirector arrays for laser ranging of satellites," NASA Technical Report NASA-TM-X-70657 (NASA Goddard Space Flight Center, 1974), available at https://ntrs.nasa.gov/archive/nasa/casi.ntrs.nasa.gov/19740018193.pdf, accessed 7/9/2019.
32. V. S. R. Gudimetla and M. J. Kavaya, "Special relativity corrections for space-based lidars," Appl. Opt. **38**, 6374–6382 (1999).
33. M. K. Barker, X. Sun, D. Mao, E. Mazarico, G. A. Neumann, M. T. Zuber, D. E. Smith, J. F. McGarry, and E. D. Hoffman, "In-flight characterization of the Lunar Orbiter Laser Altimeter instrument pointing and far-field pattern," Appl. Opt. **57**, 7702–7713 (2018).